Proceedings of the
4th JSME-KSME Thermal Engineering Conference
October 1-6, 2000, Kobe, Japan

CONTROL OF WALL SHEAR TURBULENCE WITH ARRAYED MICRO SENSOR/ACTUATOR UNITS

Takahide Endo*[1], Nobuhide Kasagi, and Yuji Suzuki

Department of Mechanical Engineering, The University of Tokyo,
Hongo 7-3-1, Bunkyo-ku, Tokyo, 113-8656, Japan

ABSTRACT

Direct numerical simulation of turbulent channel flow was made in order to evaluate feedback control with distributed micro sensors and deformable actuators. The authors has developed a new algorithm to detect quasi-streamwise vortices near the wall by using wall shear stress information only [1]. In the present study, the realizable control algorithm is applied to the drag reduction of the turbulent channel flow. Contrary to the previous turbulence control studies, each deformable actuator is assumed to have finite dimensions. The wall velocity of each actuator is determined to counteract the wall-normal velocity induced by the streamwise vortices. By the present control scheme with the arrayed sensors and actuators, 10% drag reduction is achieved through selective manipulation of the streamwise vortices and streak meandering. It is also found that the energy input of the present control is one order of magnitude smaller than the pumping power saved. High-speed region accompanied with the quasi-streamwise vortices are elevated from the wall, hence it is considered that the wall shear is attenuated with the present control.

Key Words: Wall flow, Turbulence control, Micro actuators, DNS

1. INTRODUCTION

Turbulence and concomitant phenomena such as heat transfer, diffusion, friction drag and noise play important roles in industrial and environmental problems. From the view point of saving power and protecting the environment, it is strongly desired to develop efficient turbulence control techniques for drag reduction and/or heat transfer augmentation. Among various methodologies, active feedback control attracts much attention because of its large control effect with small control input [2],[3],[4].

Since 1960's, a considerlable degree of knowledge has been accumulated on the turbulent coherent structures and their underlying mechanism (e.g., [5]). Among those coherent structures, quasi-streamwise vortices (QSV; hereafter) are known to play a dominant role in the near-wall turbulent transport phenomena [6],[7]. Jeong *et al.* [8] proposed a conceptual model of the near-wall coherent structures, which consists of a train of QSVs having alternative signs of the streamwise vorticity. They also showed that QSV tilted in the spanwise direction have close relation with the meandering of low-speed streaks, and have major contribution to the regeneration mechanism. Kravchenko *et al.* [9] showed that the streamwise vorticity accompanied with QSV has strong correlation with the wall shear stress upstream of the QSV. Kasagi & Ohtsubo [10] found that the production and destruction of the Reynolds shear stress as well as the turbulence heat flux are concentrated in the regions close to QSV.

These facts indicate that an effective control of friction drag and/or heat transfer in wall turbulence can be established through selective manipulation of QSV.

Choi *et al.* [11] investigated turbulent channel flow with local blowing/suction on the wall, which is opposite to the wall-normal velocity in the buffer layer. They obtained 30% drag reduction in their DNS, and found that QSV are attenuated. Bewley *et al.* [12] employed a suboptimal control theory [13] in order to determine the distribution of wall blowing/suction as the control input. They obtained 15% drag reduction and showed that the spatial distribution of blowing/suction determined by their suboptimal scheme is similar to that of Choi *et al.* [11].

Lee *et al.* [14] have developed a control algorithm based on neural networks. They determined the control input by using only wall variables, and found that the wall shear is substantially decreased when the blowing/suction rate is roughly proportional to the spanwise

*[1] Present address: Computer and Information Division, The Institute of Physical and Chemical Research (RIKEN), Hirosawa 2-1, Wakou-si, Saitama, 351-0198, Japan.
E-mail: tendo@postman.riken.go.jp

gradient of the spanwise shear stress. Lee *et al.* [15] proposed a suboptimal control scheme with the Fourier transformation, and showed that their control scheme by using elaborate cost function is very effective in reducing drag.

It is noted that in most previous DNS studies for controlling wall turbulence, an infinite number of sensors and actuators were assumed, and their volumes were neglected. Since this assumption is unrealistic, it is desired to develop a new control algorithm assuming arrayed sensors and actuators of finite spatial dimensions.

Devices for turbulence feedback control should have spatio-temporal scales comparable with those of the coherent structures [16]. Recent development of microelectromechanical systems (MEMS) technology enables us to fabricate prototypes of such micro devices [17]. Among various kinds of actuators, wall deformation is considered to be one of the most promising candidates, because of its robustness against the hostile environment [18].

Carlson & Lumley [19] employed a Gaussian-shaped deformable bump as an actuator in their DNS of a minimal channel flow [20]. They found that, when a bump having a maximum height of 12 viscous length and a maximum velocity of one friction velocity swells underneath the high-speed regions, the faster moving fluid is displaced away from the wall, and thus the friction drag is decreased as much as 7%. They showed thath the wall deformation is effective in modification of turbulence.

Endo *et al.* [1] employed DNS of turbulent channel flow with actively deforming walls. They showed that about 12% drag reduction is observed when the wall volocity is given to be out-of-phase of the wall-normal velocity in the buffer region. The power input for deforming walls are fairly small than the pumping power saved, and it is showed that the wall deformation is effective in turbulence control. They also showed the characteristic dimensions ow wall deformation, i.e.; about 200 and 60 viscous lengths in the streamwise and spanwise directions, respectively.

They has developed a new algorithm to detect QSV near wall by wall shear stress information. They showed that QSV is successfully captured by the spanwise gradients of wall shear stress. QSV is observed at 50 ν/u_τ downstream from the sensing location.

The objectives of the present study are to evaluate their control algorithm with arrayed wall deformable actuators for drag reduction, where the actuators have a finite dimension. And to investigate the efficiency and the mechanism of drag reduction under the present control. For this purpose, we employed DNSs of turbulent channel flow with deformable two walls.

2. NUMERICAL PROCEDURE

The flow geometry and the coordinate system are shown in Fig. 1. The governing equations are the incompressive Navier-Stokes equations and the continuity equation. Wall deformation is represented with a boundary-fitted coordinate system for moving boundary. Periodic boundary conditions are employed in the streamwise ($x-$) and spanwise ($z-$) directions, while non-slip boundary condition is imposed on the top and bottom deformable walls.

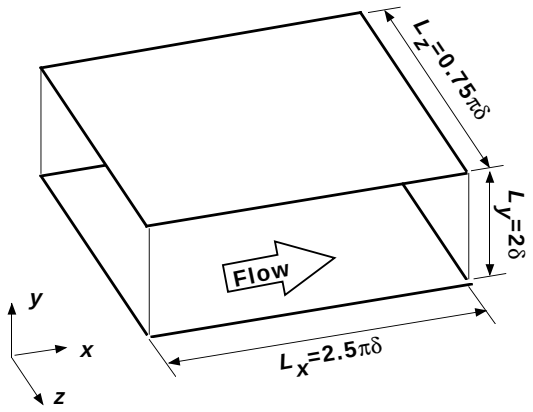

Figure 1. Flow geometry and coordinate system.

A modified Crank-Nicolson type fractional-step method [21] is used for the time advancement, while a second-order finite difference scheme is employed for the spatial discretization of both flow variables and metrics on a staggered mesh [22]. The pressure Poisson equation is solved with the multi-grid method [23].

The size of the computational volume is respectively $2.5\pi\delta$ and $0.75\pi\delta$ in the $x-$ and $z-$ directions, where δ is the channel half width. The simulation is performed under the constant flow rate condition throughout the present study. The Reynolds number based on the bulk mean velocity U_b and the channel width 2δ is 4600 (about 150 based on the wall friction velocity u_τ and δ). The computational domain is about 1180 and 360 viscous length scales in the $x-$ and $z-$ directions, respectively, which are about 2.5 and 3.6 times larger than the minimal flow unit [20]. Hereafter, $(\ )^+$ represents a quantity non-dimensionalized by the friction velocity u_τ in the plane channel flow without control and the kinematic viscosity ν.

The number of grid points is 96, 97 and 96 in the $x-, y-$ and $z-$directions, respectively. A non-uniform mesh with a hyperbolic tangent distribution is employed in the $y-$direction. The first mesh point away from the wall is given at $y^+ = 0.25$. The computational time step is chosen as $0.33\nu/u_\tau^2$. The initial condition is given from a fully-developed velocity field of preceding channel flow DNS.

3. DETECTION OF QUASI-STREAMWISE VORTEX BASED ON WALL VARIABLES

It is well known that the near-wall streaky structures do not always flow straight in the streamwise direc-

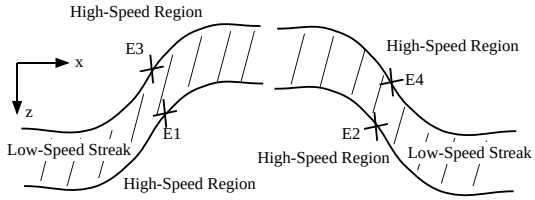

Figure 2. Schematic of a modelled streaky structure.

tion, but often meander in the spanwise direction. Johansson *et al.* [24] made a conditional average of a DNS database [25] and found that the turbulent production was very large near the streaky structures asymmetric in the spanwise direction. Hamilton *et al.* [26] pointed out that QSV and the streaky structure have close dynamical relationship with each other, and the meandering of streaks plays an important role in a quasi-cyclic process of turbulence regeneration. Jeong *et al.* [8] proposed a schematic model of QSV alternatively tilting in the $x-z$ plane associated with the meandering of the near-wall low-speed streak. From the information mentioned above, it is expected that QSV can be identified from the wall information by detecting the streak meandering.

Figure 2 shows a schematic of a modelled streaky structure. When the velocity gradients in the two horizontal directions are taken into account, the edges of the streak can be grouped into four events E1∼E4, depending on the signs of $\partial u'/\partial x$ and $\partial u'/\partial z$. Note that E1 and E4, and also E2 and E3 are respectively of mirror symmetry in the spanwise direction.

Endo *et al.* [1] investigated a conditionally averaged flow field around the meandering streaks given the condition of the combination of the signs $\partial u'/\partial x$ and $\partial u'/\partial z$ at $y^+ = 15$ using DNS database of turbulent channel flow. They showed that the QSV with strong streamwise vortices are observed at the downstream edge of low-speed streaks, i.e.; large peaks of positive and negative ω_x are observed at Events E1 and E4, respectively, while small values of ω_x are observed at Events E2 and E3.

They also showed that the spanwise gradients of τ_u^+ ($\equiv \partial u'^+/\partial y^+|_w$) and τ_w^+ ($\equiv \partial w'^+/\partial y^+|_w$) instead of the velocity gradients in the buffer layer are good indicators for the meandering streaks. The signs of the shear stress gradients and the corresponding events are summarized in Table 1. A negative value of $\partial\tau_w/\partial z$ is observed $50\nu/u_\tau$ upstream of Events E1 and E4, while $\partial\tau_w/\partial z > 0$ for E2 and E3. Note that Event E1 can be distinguished from E4 by the sign of $\partial\tau_u/\partial z$ at the same location.

Figure 3 shows the contours of the streamwise velocity fluctuation $< u'^+ >$ at $y^+ = 15$, conditionally averaged for S1 ($\partial\tau_u^+/\partial z^+ > 0.035$ and $\partial\tau_w^+/\partial z^+ < -0.005$). The meandering of the low-speed streak corresponding to E1 is well captured at $50\nu/u_\tau$ downstream from the detection point. A large positive peak of ω_x^+ at $y^+ = 15$ is also observed in the same region, where the streak meanders as shown in Fig. 4. Although it is not shown

Table 1. Four signals and corresponding events.

Signal	$\partial\tau_u/\partial z$	$\partial\tau_w/\partial z$	Event	ω_x'
S1	Positive	Negative	E1	Positive
S2	Positive	Positive	E2	
S3	Negative	Positive	E3	
S4	Negative	Negative	E4	Negative

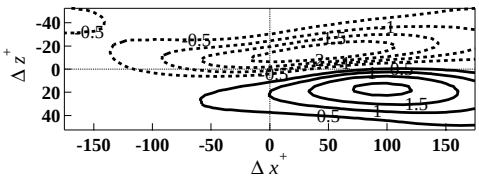

Figure 3. Contours of streamwise velocity at $y^+ = 15$, given the conditions of $\partial\tau_u^+/\partial z^+ > 0.035$ and $\partial\tau_w^+/\partial z^+ < -0.005$.

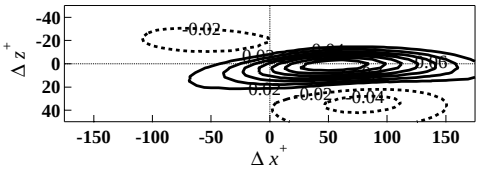

Figure 4. Contours of streamwise vorticity at $y^+ = 15$, given the conditions of $\partial\tau_u^+/\partial z^+ > 0.035$ and $\partial\tau_w^+/\partial z^+ < -0.005$.

here, a large negative peak of ω_x^+ is associated with S4 ($\partial\tau_u^+/\partial z^+ < -0.035$ and $\partial\tau_w^+/\partial z^+ < -0.005$), which corresponds to Event E4. Thus, QSV as well as its direction of rotation can be detected by the combination of the signs of $\partial\tau_u^+/\partial z^+$ and $\partial\tau_w^+/\partial z^+$.

Figure 5 shows contours of the conditionally averaged wall-normal velocity $< v'^+ >$ at $y^+ = 15$ for S1. Positive and negative peaks are aligned side-by-side in the spanwise direction, and they respectively correspond to the ejection and sweep motions. The spanwise distance of the positive and negative peaks is about $30\nu/u_\tau$, which is almost the same as the mean diameter of QSV [6].

It is noted that the present control scheme based on the dynamics of the near-wall coherent structure is similar to the algorithm by Lee *et al.* [14],[15] in the sense that it requires $\partial\tau_w/\partial z$, although they employ different schemes such as a suboptimal control scheme and an adaptive control method based on neural network. The main difference of the present scheme and their algorithm is the locations of the sensor and the actuator, i.e.; in the present scheme, the sensor and the actuator is separated around $50\nu/u_\tau$ in the streamwise direction, while they are the same location in the algorithm proposed by Lee *et al.* [14],[15].

4. FEEDBACK CONTROL WITH ARRAYED

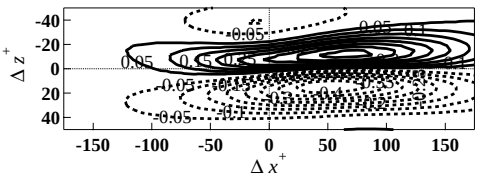

Figure 5. Contours of wall-normal velocity at $y^+ = 15$, given the conditions of $\partial\tau_u^+/\partial z^+ > 0.035$ and $\partial\tau_w^+/\partial z^+ < -0.005$.

(a)

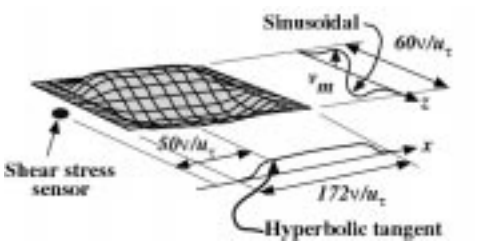

(b)

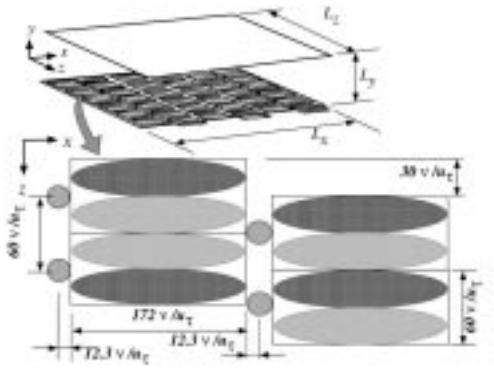

Figure 6. Schematic of arrayed actuators and shear stress sensors. (a) Dimension of a single deformable actuator. (b) Arrangement of the actuators and the sensors.

DEFORMABLE ACTUATORS

In previous studies, sensors and actuators are assumed to be infinitely small, and placed at each computational grid point on the wall. In the present study, we assume control devices having finite dimensions, and design arrayed actuators and sensors based on the discussion descrived above.

Figure 6 (a) shows a schematic of deformable actuator assumed in the present computation. By taking into account the characteristic length of the wall deformation [1], the streamwise and spanwise dimensions of the actuator is chosen as 172 and $60\nu/u_\tau$, respectively. Each actuator is assumed to be deformed only in the $y-$direction. The shape is determined with a sinusoid in the spanwise direction, in such a way that the distance between the peak and trough is about the mean diameter of QSV.

Figure 6 (b) shows an arrangement of arrayed shear stress sensors and deformable actuators. A shear stress sensor is assumed to be centered at $12.3\nu/u_\tau$ upstream from the upstream end of the deformable actuator. Hence, the streamwise distance between the sensor and the center of the actuator is $50\nu/u_\tau$, which corresponds to the displacement between the detection point of Events E1 and E4, and the peak of the streamwise vorticity shown in Fig. 4. In the present study, 36 actuators (6×6 in the streamwise and spanwise directions) are distributed with a regular pitch on both walls of the channel.

Each sensor measures the spanwise gradients of the instantaneous wall shear stresses, $\partial\tau_u/\partial z$ and $\partial\tau_w/\partial z$. The wall velocity at the center of the peak/trough of the actuator v_m is determined by:

$$v_m^+(t_{n+1}) = \begin{cases} \alpha \tanh\left(\dfrac{\partial\tau_u^+(t_n)}{\partial z^+}/\beta\right) - \gamma y_m^+(t_n), \\ \qquad\qquad \text{if } \dfrac{\partial\tau_w(t_n)}{\partial z} < 0, \\ -\gamma y_m^+(t_n), \quad \text{otherwise}, \end{cases} \tag{1}$$

where y_m is the wall displacement at the peak/trough, and α, β, and γ are control parameters, respectively. The wall velocity of each grid point on the actuator is given by

$$\begin{aligned} v_w^+(t_{n+1}) &= v_m^+(t_{n+1}) \cdot f(x^+) \cdot \exp\left[-\frac{(z^+ - z_c^+)^2}{\sigma_z^{+2}}\right] \\ &\quad \cdot \sin\left[\frac{2\pi\,(z^+ - z_c^+)}{m_z^+}\right], \end{aligned} \tag{2}$$

where the function $f(x^+)$ is introduced to keep the shape of the actuator smooth in the streamwise direction. The function f is determined with a hyperbolic tangent as:

$$f(x^+) = \begin{cases} \frac{1}{2}\left[1 + \tanh\left\{\frac{(x^+ - x_c^+) + 73.7}{\sigma_x^+}\right\}\right] \\ \qquad \cdots \text{if } -86 \le x^+ - x_c^+ \le -61.5, \\ 1 \qquad \cdots \text{if } -61.5 \le x^+ - x_c^+ \le 61.5, \\ \frac{1}{2}\left[1 - \tanh\left\{\frac{(x^+ - x_c^+) - 73.7}{\sigma_x^+}\right\}\right] \\ \qquad \cdots \text{if } 61.5 \le x^+ - x_c^+ \le 86. \end{cases} \tag{3}$$

In Eqs. (4) and (5), x_c and z_c denote the location of the center of the actuator. The parameters are somewhat tuned through preliminary computations, and chosen as $\alpha = 2.3, \beta = 0.077, \gamma = 0.3, \sigma_x^+ = 6.14$, and $\sigma_z^+ = 22.2$, respectively.

Figure 7 shows a time trace of the normalized pressure drop for the cases of local blowing/suction [11] and the continuous wall deformation [1]. It is seen the drag is gradually decreased from the onset of the control. The present result, however, exhibits no control effect until $t^+ = 200$, and then the drag is decreased at $t^+ > 200$. A maximum drag reduction rate of 17% is obtained at $t^+ = 800$. Therefore, even with coarsely distributed sensors and actuators on the wall, the effect of the present control scheme appears to be efficient through selective manipulation of QSV.

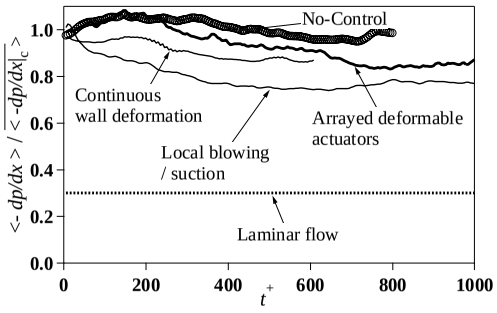

Figure 7. Time trace of the normalized mean pressure gradient.

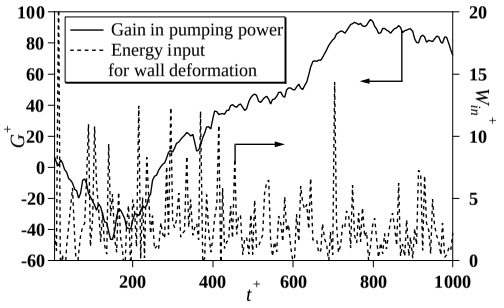

Figure 8. The gain in pumping work and the energy input.

The gain in pumping power G and the energy input to deform actuators W_{in} are calculated to evaluate the performance of the present control. After Mito & Kasagi [22], (i) work of convecting of turbulent kinematic energy, (ii) pressure work, and (iii) stress work, are taken into account as energy input, although the work for stretching the wall material is neglected.

$$G = \left[\left(-\overline{\frac{\partial p}{\partial x}}\right)_{\text{No-control}} - \left(-\frac{\partial p}{\partial x}\right)_{\text{Control}}\right] \cdot Q, \quad (4)$$

$$W_{in} = \int_{\Gamma_w} \left[\underbrace{p'_w \cdot v_n}_{\text{(i)}} + \underbrace{k \cdot v_n}_{\text{(ii)}} + \underbrace{\left(-\frac{1}{Re}\frac{\partial k}{\partial n}\right)}_{\text{(iii)}}\right] d\Gamma_w, \quad (5)$$

where Q, k and p'_w denote the flow rate, turbulent kinetic energy, and wall pressure fluctuation, respectively. The subscript n denotes wall-normal direction, and Eq. (7) is the surface integration over the deformable wall.

As shown in Fig. 8, the energy input for deforming actuators are much smaller than the pumping power saved. The mean efficiency $\eta(\equiv G/W_{in})$ is on the order of 10, and this fact demonstrates that the efficiency of the present control scheme with arrayed deformable actuators can be markedly large.

Figure 9 shows the top views of instantaneous flow fields at $t^+ = 0$ and 604. Vortical structures are identified with their negative value of the second invariant of the deformation tensor ($II' = u'_{i,j}u'_{j,i}$) [27],[[7]. Under

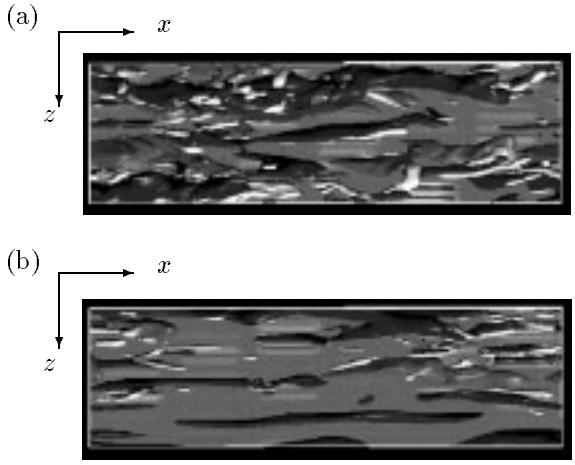

Figure 9. Top view of the instantaneous flow field. Flow: left to right. White: $II'^+ = -0.03$, Dark grey: $u'^+ = -3.5$, Light grey: $u'^+ = 3.5$. (a) $t^+ = 0$, (b) $t^+ = 604$.

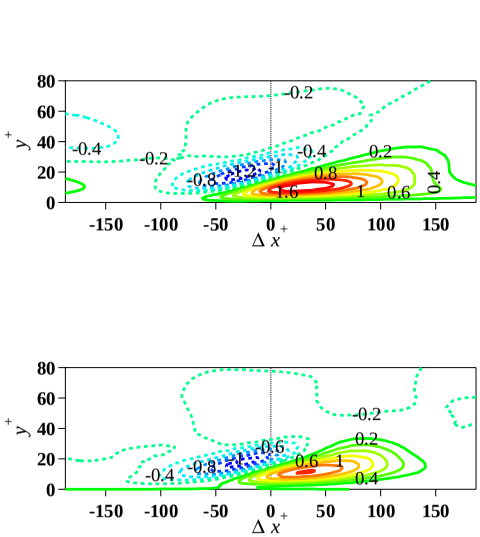

Figure 10. Conditionally averaged streamwise velocity fluctuation on the $x-y$ plane given the condition of $II'^+ = -0.03$ at $y^+ = 15$. (a) No-Control, (b) Control.

the present control with deformable actuators, QSV becomes less populated near the wall and the meandering of low-speed streak is surpressed.

Figures 10 (a), (b) show the conditionally averaged streamwise velocity fluctuation $< u'^+ >$ on the $x-y$ plane, given the condition of $II'^+ = -0.01$ at $y^+ = 15$. Note that the spanwise axis is reversed depending on the sign of the ω_x at the detection point. Solid lines correspond to the high-speed region while dashed lines represent the low-speed streaks. High- and low-speed streaks accompanied with the QSV have negative and positive wall normal velocity, which correspond to the sweep and ejection events, respectively. High-speed region is comparatively suppressed and is slightly elevated away from the wall under the control, hence the high wall shear region is suppressed. On the other hand, low-speed streak stays near wall region, thus the ejection event should be

attenuated.

6. CONCLUSIONS

A new simple control scheme using only wall variables is evaluated with distributed sensors/deformable actuators in direct numerical simulation of turbulent channel flow. About 10% drag reduction is achieved. This fact shows a realizable control is expected through selective manipulation of QSV, although micro sensors/actuators are distributed rather coarsely on the wall. The streamwise vortices and streak meandering are selectively attenuated by the present control scheme. And the energy input of the present control is one order of magnitude smaller than the pumping power saved. Owing to the present control with deformable actuators, high-spped region accompanied with the sweep event is elevated from the wall, while low-speed streak remains near-wall region.

References

[1]Endo, T., Kasagi, N., and Suzuki, Y., 1999, "Feedback Control of Wall Turbulence with Wall Deformation," 1st Int. Symp. Turbulece & Shear Flow Pheonomena, Santa Barbara, pp. 405-410.

[2] Moin, P., and Bewley, T., 1994, "Feedback control of turbulence," Appl. Mech. Rev., Vol. 47, S3-S13.

[3]Gad-el-Hak, M., 1996, "Modern developments in flow control," Appl. Mech. Rev., Vol. 49, pp. 365-377.

[4]Kasagi, N., 1998, "Progress in direct numerical simulation of turbulent transport and its control," Int. J. Heat & Fluid Flow, Vol. 19, pp. 125-134.

[5]Cantwell, B. J., 1981, "Organized motion in turbulent fnlow," Ann. Rev. Fluid Mech., Vol. 13, pp. 457-515.

[6]Robinson, S.K., 1991, "Coherent motions in the turbulent boundary layer," Annu. Rev. Fluid Mech., Vol. 23, pp. 601-639.

[7]Kasagi, N., Sumitani, Y., Suzuki, Y., and Iida, O., 1995, "Kinematics of the quasi-coherent vortical structure in near-wall turbulence," Int. J. Heat & Fluid Flow, Vol. 16, pp. 2-10.

[8]Jeong, J., Hussain, F., Schoppa, W., and Kim, J., 1997, "Coherent structures near the wall in a turbulent channel flow," J. Fluid Mech., Vol. 332, pp. 185-214.

[9]Kravchenko, A. G., Choi, H., and Moin, P., 1993, "On the relation of near-wall streamwise vortices to wall skin friction in turbulent boundary layers," Phys. Fluids A, Vol. 5, No. 12, pp. 3307-3309.

[10]Kasagi, N., and Ohtsubo, Y., 1992, "Direct numerical simulation of low Prandtl number thermal field in a turbulent channel flow," Turbulent Shear Flows 8, Durst *et al.* eds., Springer-Verlag, Berlin, pp. 97-119.

[11]Choi, H., Moin, P., and Kim, J., 1994, "Active turbulence control for drag reduction in wall-bounded flows," J. Fluid Mech., Vol. 262, pp. 75-110.

[12]Bewley, T.R., Choi, H., Temam R., and Moin P., 1993, "Optimal feedback control of turbulent channel flow," CTR Annual Research Briefs, Stanford Univ., pp. 3-14.

[13]Choi, H., Temam, R., Moin, P., & Kim, J., 1993, "Feedback control for unsteady flow and its application to the stochastic Burgers equation," J. Fluid Mech., Vol. 253, pp. 509-543.

[14]Lee, C., Kim, J., Babcock, B., and Goodman, R., 1997, "Application of neural networks to turbulence control for drag reduction," Phys. Fluids, Vol. 9, pp. 1740-1747.

[15]Lee, C., Kim, J., and Choi, H., 1998, "Suboptimal control of turbulent channel flow for drag reduction," J. Fluid Mech., Vol. 358, pp. 245-258.

[16]Gad-el-Hak, M., 1994, "Interactive Control of Turbulent Boundary Layers: A Futuristic Overview," AIAA J., Vol. 32, No. 9, pp. 1753-1765.

[17]Ho, C-M., and Tai, Y-C., 1996, "Review: MEMS and Its Applications for Flow Control," ASME J. Fluids Eng., Vol. 118, pp. 437-447.

[18]Grosjean, C., Lee, G. B., Hong, W., Tai, Y.-C., and Ho, C.-M., 1998, "Micro Ballon Actuators for Aerodynamic Control," Proc. 11th MEMS Workshop, pp. 166-171.

[19]Carlson, H.A., & Lumly, J.L., 1996, "Active control in the turbulent wall layer of a minimal flow unit," J. Fluid Mech., Vol. 329, pp. 341-371.

[20]Jiménez, J., and Moin, P., 1991, "The minimal flow unit in near-wall turbulence," J. Fluid Mech., Vol. 225, pp. 213-240.

[21]Choi, H., and Moin, P., 1994, "Effects of the computational time step on numerical solutions of turbulent flow," J. Comput. Phys. Vol 113, pp. 1-4.

[22]Mito, Y., and Kasagi, N., 1998, "DNS study of turbulence modification with streamwise-uniform sinusoidal wall-oscillation," Int. J. Heat & Fluid Flow, Vol 19, pp. 470-481.

[23]Demuren, A.O., and Ibraheem, S.O., 1998, "Multigrid method for the Euler and Navier-Stokes equations," AIAA J., Vol. 36, pp. 31-37.

[24]Johanson, A.V., Alfredsson, P.H., and Kim, J., 1991, "Evolution and dynamics of shear-layer structures in near-wall turbulence," J. Fluid Mech., Vol. 224, pp. 579-599.

[25]Kim, J., Moin, P., and Moser, R., 1987, "Turbulence statistics in fully developed channel flow at low Reynolds number," J. Fluid Mech., Vol. 177, pp. 133-166.

[26]Hamilton, J. M., Kim, J., and Waleffe, F., 1995, "Regeneration mechanism of near-wall turbulence structures," J. Fluid Mech., Vol. 287, pp. 317-348.

[27]Chong, M. S., Perry, A. E., & Cantwell, B. J., 1990, "A general classification of three dimensional flow fields," Phys. Fluids A, Vol. 2, No. 5, pp. 765-777.